Field Ionization and Field Emission with Intense, Single-cycle THz Pulses
Need to replace with my own title

by

© Yunxiao Wang

A thesis submitted to the

School of Graduate Studies

in partial fulfilment of the

requirements for the degree of

Anqing, Anhui, China

B.S. in Physics University of Science and Technology of China May 2009

Memorial University of Newfoundland

Doctor of Philosophy

St. John's Newfoundland

Department of Physics August, 2016

Abstract

Nuclear-polarized ^{3}He targets have been widely used in electron-scattering experiments in Thomas Jefferson National Accelerator Facility (JLAB) since mid 1990s. It is of great importance to produce large amounts of ^{3}He gas with high polarization.

The latest experiments run in JLAB prior to the 12GeV upgrade have been using cells polarized with Spin-Exchange Optical Pumping (SEOP). These cells were made of the GE180 glass and use a two-chambered design. The top chamber, known as the pumping chamber, is where ^{3}He is polarized through SEOP. The bottom chamber, known as the target chamber, is where electron scattering occurs. Great effort has been made in our lab to develop this generation of cells. Alkali-hybrid SEOP together with narrowband laser diode arrays have increased the ^{3}He polarization from 37% to 65%. Among other things, we also carefully studied an additional spin relaxation mechanism that limits the maximum achievable ^{3}He polarization.

The 12GeV upgrade makes the future experiments much more demanding in terms of target cell performance. One challenge it brings is the high relaxation due to electron beam. We have designed and tested a new style cell that uses convection instead of diffusion to increase the rate at which the polarization in the target chamber is being replenished by gas from pumping chamber. We have obtained over 50% polarization with controllable convection speed so far.

An additional problem that comes with higher beam current is that the glass end windows of traditional design are not likely to survive the experiments. Our group started exploring the option of using metal end windows from a decade ago. The first problem to solve is to find out the correct material and the proper technique

to incorporate metal without introducing significant spin relaxation and still being able to hold high pressure gas (12 atm) inside. This is a brand new technique that may have a profound impact of future cell designs once fully developed. Although no metal end windows have been tested so far, multiple glass cells with different kinds metal tubes (much larger in area compared to the end windows that will be used in JLAB experiments) attached were examined and were enough to convince us the extra spin relaxation is not likely to cause significant problems. The metals tubes were connected to Pyrex glass with knife-edge (housekeeper) seals and stayed intact through high pressure tests. After exploring options such as pure copper, gold coated copper, titanium, stainless steel, gold coated titanium, we have established that electroplating gold on copper substrate yields the best result so far. Further tests are planned before attaching metal end windows to GE180 glass and using them in electron-scattering experiments.

Acknowledgements

Put your acknowledgements here...

"Intellectual and practical assistance, advice, encouragement and sources of monetary support should be acknowledged. It is appropriate to acknowledge the prior publication of any material included in the thesis either in this section or in the introductory chapter of the thesis."

— MUN School of Graduate Studies

Contents

List of Tables

List of Figures

Chapter 1

^{3}He Polarimetry

1.1 Overview

Historically, pure-glass target cells used in electron scattering experiments have been studied mainly using Adiabatic Fast Passage (AFP) [**?**] Nuclear Magnetic Resonance (NMR) and Electron Paramagnetic Resonance (EPR) [**?**]. AFP is a technique that allows us to monitor a signal that is directly proportional to the ^{3}He polarization, which serves as a means to gain knowledge of properties of cell including the time it takes to polarize it and the relaxation rates of its polarization. The EPR technique utilizes the fact that polarized ^{3}He produces frequency shift of the magnetic resonance lines of alkali metal to measure the ^{3}He polarization. When AFP and EPR are combined, we can calculate the calibration constant between an AFP signal and the corresponding ^{3}He polarization.

A significant focus of my studies was on exploring cells that incorporated metal. Unfortunately, AFP is not suitable for studying such cells as it requires exposing the

entirety of the cell to a Radio Frequency (RF) magnetic field in an attempt to flip all spins in the cell more-or-less simultaneously. The RF field would induce Eddy currents in the metal portions of the cell that would significantly affect the resulting signal. For glass and metal cells, Pulsed Nuclear Magnetic Resonance (PNMR) has proven to be very useful. Using PNMR, it is possible to apply the RF field to a small selected part of the cell which makes it relatively easy to prevent metal from distorting the signal.

This chapter introduces the three techniques mentioned above and how they're used for our studies.

1.2 Adiabatic Fast Passage

1.2.1 Nuclear Magnetic Resonance

The energy of a magnetic moment in an external field is

$$E = -\vec{\mu} \cdot \vec{B_0} = -\mu_z B_0 \tag{1.1}$$

where $\vec{\mu}$ is the magnetic moment. For a spin-1/2 nuclei, the energy is

$$E = -\gamma B_0 \hbar/2 \tag{1.2}$$

where γ is the gyromagnetic ratio, and $\gamma/2\pi \approx 3.2434\,\mathrm{kHz/Gauss}$. When a nucleus is placed in an external magnetic field that is not aligned with its magnetic moment, it will precess at the Larmor frequency. The Larmor frequency is defined as $\omega = \gamma B_0$.

1.2.2 The Rotating Coordinate System

1.2.2.1 Classical Formulation

For a nucleus in an external field $\vec{B}$ with $\gamma\hbar\vec{I}$ as its nuclear angular momentum, the equation of motion in a stationary coordinate system is [**?**]

$$\hbar\frac{d\vec{I}}{dt} = \gamma\hbar\vec{I} \times \vec{B}. \tag{1.3}$$

Let $\frac{\partial}{\partial t}$ represent the derivative with respect to a coordinate system that rotates with angular velocity $\vec{\omega}$, then

$$\frac{d\vec{I}}{dt} = \frac{\partial\vec{I}}{\partial t} + \vec{\omega} \times \vec{I}. \tag{1.4}$$

Substitute Eq. 1.4 into Eq. 1.3, $\vec{I}$ in the rotating frame satisfies the equation of motion

$$\hbar\frac{\partial\vec{I}}{\partial t} = \gamma\hbar\vec{I} \times (\vec{B} + \vec{\omega}/\gamma) = \gamma\hbar\vec{I} \times \vec{B_{eff}} \tag{1.5}$$

where $\vec{B_{eff}}$ is the effective field in the rotating frame

$$\vec{B_{eff}} = \vec{B} + \vec{\omega}/\gamma \tag{1.6}$$

Thus, the effective field experienced by an observer in the rotating frame is simply the external field $\vec{B}$ plus an additional field $\vec{\omega}/\gamma$.

If we apply this result to rotating magnetic fields, we will get the core idea of performing an Adiabatic Fast Passage (AFP) measurement. Assuming a constant field $\vec{B}$ and another field $\vec{B_1}$ perpendicular to $\vec{B}$ that is rotating with angular velocity

$-\omega$. In the rotating frame that rotates with $\vec{B_1}$, both aforementioned fields are just constant and the effective field in the rotating frame is

$$B_{eff}\vec{z} = (B - \omega/\gamma)\vec{z} + B_1\vec{x'} \tag{1.7}$$

where $\vec{x'}$ is the direction that $\vec{B_1}$ is in. When on resonance (B = ω/γ), the effective field is perpendicular to the constant field $\vec{B}$.

1.2.2.2 Quantum Mechanical Formulation

The above conclusion can be easily reached with quantum mechanics [**?**]. The Shrödinger equation for a magnetic moment in an external field is

$$i\hbar\dot{\psi} = \mathcal{H}\psi = -\gamma\hbar\vec{I}\cdot\vec{B}\psi. \tag{1.8}$$

Let ψ and $\vec{B}$ be the wave function and magnetic field respectively in a stationary frame and ψ_r and $\vec{B_r}$ be the same quantities in a rotating frame with angular velocity $\vec{\omega}$. Using the rotation operator in quantum mechanics,

$$\psi = e^{-i\vec{\omega}\cdot\vec{I}t}\psi_r \tag{1.9a}$$

$$\vec{I}\cdot\vec{B_r} = e^{i\vec{\omega}\cdot\vec{I}t}\vec{I}\cdot\vec{B}e^{-i\vec{\omega}\cdot\vec{I}t} \tag{1.9b}$$

Substituting 1.9 into Eq.1.8, the Shrödinger equation in the rotating frame is obtained

$$i\hbar\dot{\psi_r} = -\gamma\hbar\vec{I}\cdot(\vec{B_r} + \vec{\omega}/\gamma)\psi_r = -\gamma\hbar\vec{I}\cdot\vec{B_{eff}}\psi_r \tag{1.10}$$

The same effective field in the rotating frame is reached as that from the classical derivation.

1.2.3 Adiabatic Fast Passage

The NMR technique of Adiabatic Fast Passage (AFP) is used to measure the ^{3}He polarization. In an AFP measurement, with the assistance of an oscillating radiofrequency (RF) field, the spins follow the effective field in a rotating frame (as discussed in more detail below) and are flipped 180 degrees to the opposite direction and then flipped back, producing two peaks in signal when they're perpendicular to the holding field and the pick up coils.

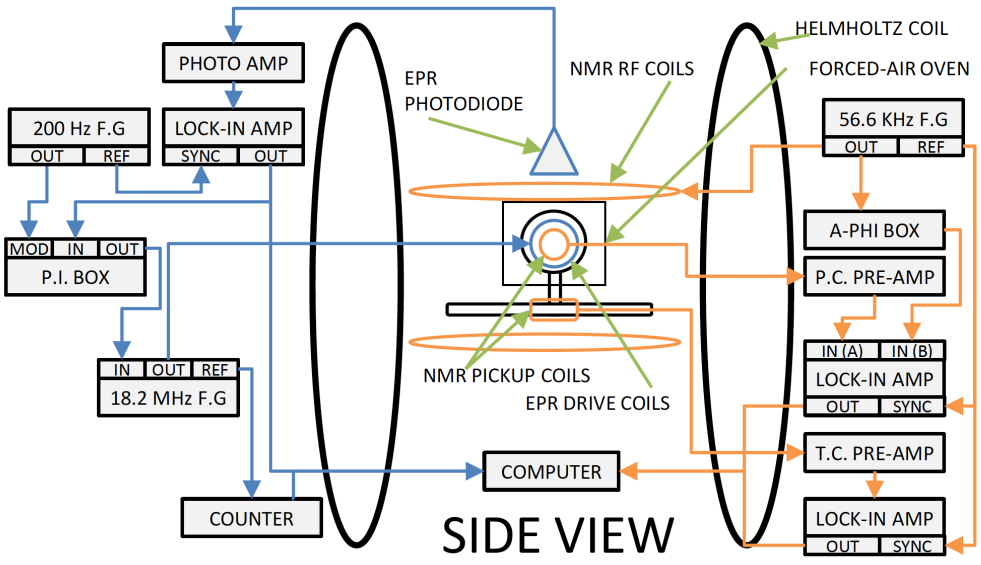

Figure 1.1: EPR (left) and AFP (right) setup. Adapted from Dolph's PhD thesis.

The flipping process can be achieved by either sweeping the main holding field or sweeping the RF frequency so that the longitudinal component of effective field in the rotating frame goes through zero. AFP measurements in our lab were typically done by sweeping the holding field while keeping the RF frequency constant. The RF coils produced an RF field of magnitude $2B_1$ perpendicular to the main holding field B. The oscillating field has a frequency of ω and can be decomposed into two counter-rotating components with the same amplitude B_1. Only the component rotating in the direction able to produce a resonance in Eq. 1.7 has an important effect. In this frame, the effective field is

$$\vec{B_{eff}} = (B - \omega/\gamma)\vec{z} + B_1\vec{x'} \tag{1.11}$$

as discussed above. The other rotating component that rotates in the opposite direction does not affect the spins. In an AFP measurement, the holding field starts from a value lower than ω/γ ($\omega/\gamma - B \gg B_1$), so that, initially, the effective field is almost aligned with the holding field and the spins. The holding field is then swept at a constant rate through resonance to a value greater than ω/γ. The sweeping rate is of great importance. The sweep needs to be slow enough so that the nuclear spins can follow the effective field

$$\frac{\dot{B}}{B_1} \ll \omega \tag{1.12}$$

Sweep rates that satisfy this condition are considered to be adiabatic.

Sweep rates cannot be too slow either, because the relaxation rate of the spins are faster near the resonance especially with a small effective field B_1. The relaxation

rate of ^{3}He in the rotating frame due to magnetic field inhomogeneities at resonance is [?]

$$\frac{1}{T_{1r}} = D\frac{|\nabla B_z|^2}{B_1^2} \tag{1.13}$$

where D is the ^{3}He self-diffusion constant. In order to keep the AFP loss low, it's important for the time scale during which the spins are close to resonance to be much shorter than T_{1r}, so we want:

$$D\frac{|\nabla B_z|^2}{B_1^2} \ll \frac{\dot{B}}{B_1} \tag{1.14}$$

In the work presented here, the field was typically swept from 12.6 Gauss to 20.4 Gauss in 6s, thus

$$\dot{B} = 1.3G/s \tag{1.15a}$$

$$B1 \approx 100mG \tag{1.15b}$$

$$f = 56.6kHz \tag{1.15c}$$

$$D \approx 0.16cm^2/s \tag{1.15d}$$

$$|\nabla B_z| \approx 10mG/cm \tag{1.15e}$$

$$\tag{1.15f}$$

With these operating conditions,

$$D\frac{|\nabla B_z|^2}{B_1^2} \approx 1.6mHz \tag{1.16a}$$

$$\frac{\dot{B}}{B_1} \approx 13Hz \tag{1.16b}$$

$$\omega \approx 356kHz \tag{1.16c}$$

The AFP conditions were clearly well satisfied for our parameters. Fig.1.2 shows the evolution of effective field in the rotating frame during an AFP measurement.

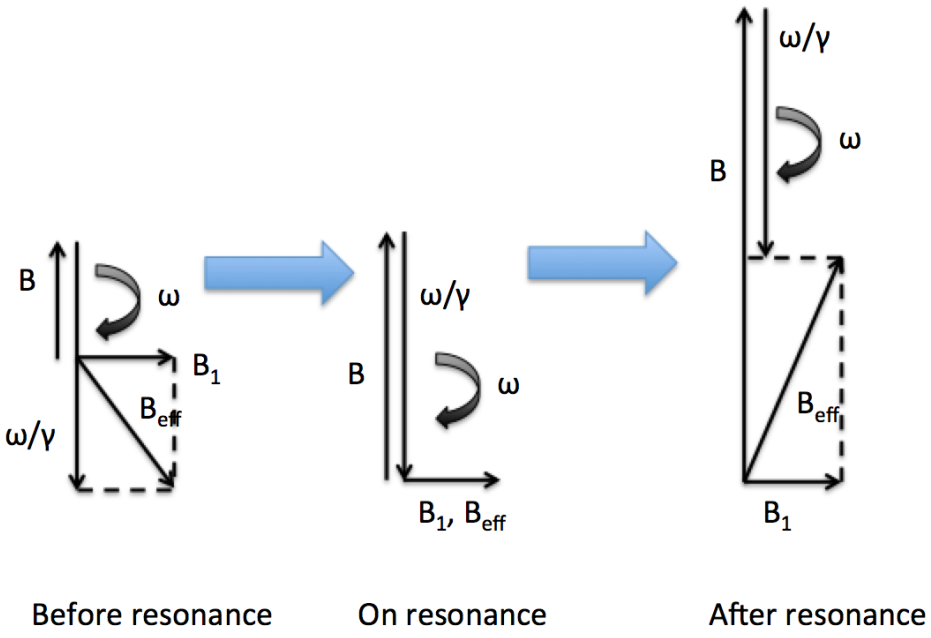

Figure 1.2: Effective field in the rotating frame during an Adiabatic Fast Passage measurement. The ^{3}He spins follow the direction of the effective field. B_1 is exaggerated to show different components of effective field clearly.

During our AFP measurements, the pick up coils were placed close to the cell, with their axis perpendicular to both the holding field and RF field. Under these conditions, as the ^{3}He spins precess along the holding field, the transverse component of the spins induces an electromotive force (EMF) that is directly proportional to the amplitude of the component in the pick up coils. The resulting signal can be written as:

$$S = A\omega \sin\alpha(t) = A\omega \frac{B_1}{\sqrt{B_1^2 + (B(t) - \omega/\gamma)^2}} \tag{1.17}$$

where A is a constant that accounts for the cell and coils geometry, the cell magnetization and the electronics factors that affect the size of signal; ω is the RF frequency; α is the angle between the effective field and the holding field in the rotating frame; B(t) is the holding field as a function of time. The signal reaches peak value when $B(t) = \omega/\gamma$. Fig.1.3 shows the result of a typical AFP measurement.

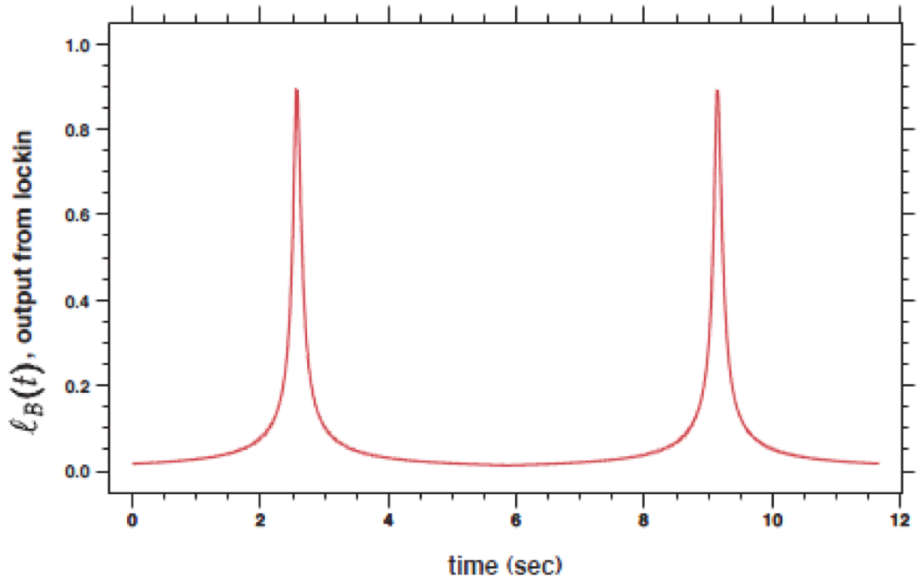

Figure 1.3: A typical AFP signal. y axis is in arbitrary unit.

1.2.4 AFP Loss

The longitudinal spin relaxation rate due to static field inhomogeneities is [**?**, **?**, **?**]

$$\frac{1}{T_1} = D\frac{|\nabla B_x|^2 + |\nabla B_y|^2}{B_0^2} \tag{1.18}$$

where D is the diffusion constant for the polarized spins, and is inversely proportional to the gas pressure. B_0 is the mean magnetic field along z axis. B_x and B_y are the x and y components of the magnetic field. However, when performing AFP measurement, the spins are exposed to a small oscillating RF field, the spin relaxation can be greatly accelerated under magnetic resonance conditions [**?**],

$$\frac{1}{T_{r1}} = \frac{8R^4}{175D}|\nabla\Omega_z|^2 \sum_n \frac{175}{4(\chi_{1n}^2 - 2)(\chi_{1n}^4 + r^2 + r^2 s^2)(1 + s^2)} \tag{1.19}$$

where R is the cell radius, D is the diffusion constant, Ω_z is the Larmor frequency of the holding field, $r = \frac{\omega_r R^2}{D}$, $s = \frac{\Omega_0 - \omega}{\omega_r}$, and the numbers χ_{1n} are the zeros of the derivatives of the spherical Bessel functions

$$\frac{d}{dx} j_1(x_{1n}) = 0 \; for \; n = 1, 2, 3... \tag{1.20}$$

Since $r^2 \gg \chi_{1n}^4$, and $\sum_n \frac{1}{\chi_{1n}^2 - 2} = \frac{1}{2}$ [**?**],

$$\frac{1}{T_{r1}} = \frac{R^4|\nabla\Omega_z|^2}{r^2(1 + s^2)^2 D} = \frac{|\nabla B_z|^2 D}{B_1^2(1 + s^2)^2} \tag{1.21}$$

If P_0 is the polarization before AFP, the polarization P after a single AFP flip is given by

$$P = P_0 e^{-\int \Gamma_{r1} dt} = P_0 e^{-\int \frac{1}{T_{r1}} dt} \tag{1.22}$$

Thus fraction loss L_{AFP} due to a single AFP flip is:

$$L_{AFP} = 1 - e^{\int \frac{1}{T_{r1}} dt} \approx \int \frac{1}{T_{r1}} dt \tag{1.23}$$

For our conditions, the integration limits can be extended to $\pm\infty$, making it possible to calculate the integral as:

$$\int_{-\infty}^{\infty} \frac{1}{T_{r1}} dt = \frac{\pi D|\nabla B_z|^2}{2B_1 \partial B_1/\partial t} \tag{1.24}$$

which is the fractional loss due to a single AFP flip.

To better understand AFP loss, we performed a study where we took AFP measurements at various different field gradients to study the relation between AFP loss and inhomogeneities. The gradients were produced by Maxwell-style transverse gradient coils and increased from 0 to a little under 160 mG/cm. At each set gradient, we take one AFP to look at the difference between the two peaks to determine the loss due to a single flip. Fig 1.4 shows AFP losses collected from experiments and theoretical predictions. They agree within the error bar.

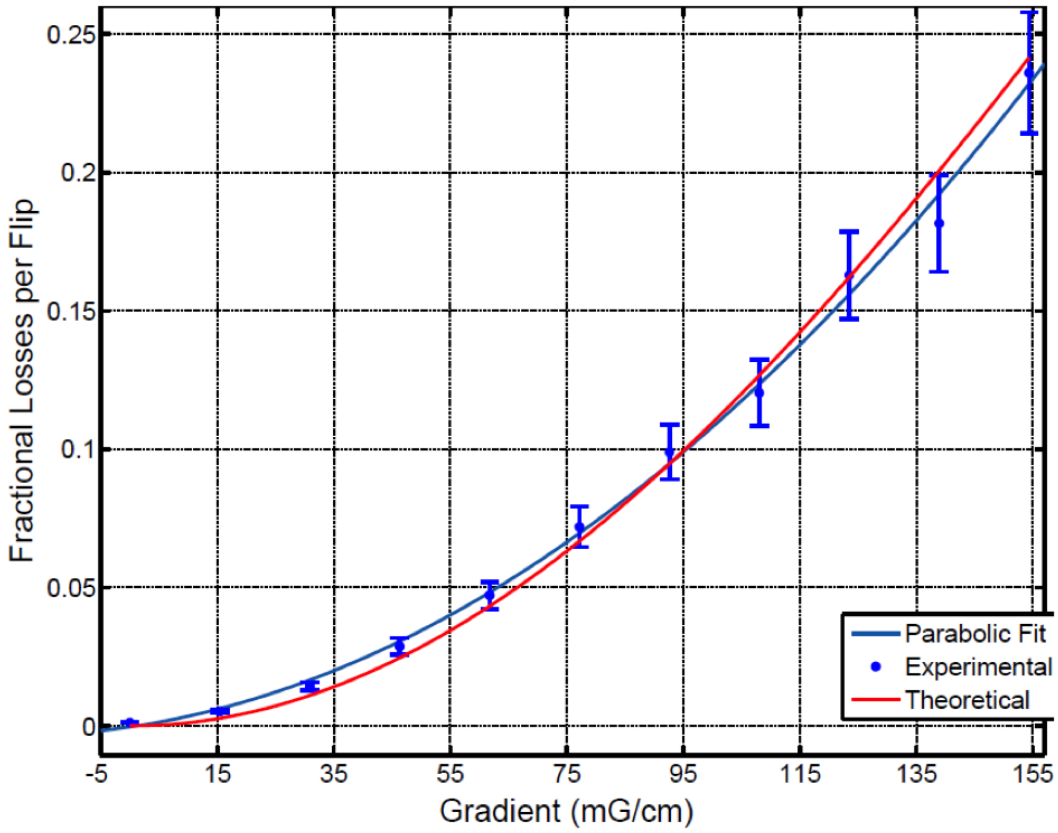

Figure 1.4: Fractional AFP loss (single flip) as a function of field gradient.

1.3 Electron Paramagnetic Resonance

1.3.1 Overview

Electron Paramagnetic Resonance (EPR) provides an important technique for measuring the frequency shift of alkali metal Zeeman resonances due to the effective magnetic field produced by polarized ^{3}He gas. During spin-exchange collisions, the alkali valence electron is essentially located within the ^{3}He nucleus thus facilitating a Fermi contact interaction between their spins. The EPR shift is largely caused by this Fermi-contact interaction α $\mathbf{K}\cdot\mathbf{S}$ between the nuclear spin $\mathbf{K}$ of the noble gas nucleus of magnetic moment μ_K and the electron spin $\mathbf{S}$ of the alkali metal atom [**?**]. The magnetic field created by the bulk magnetization of the ^{3}He gas also contributes directly to a relatively small part of the shift (rougly 1/6 for K). Because the spin-exchange effective field is difficult to calculate accurately from theory, the total measured shift is usually written as the expected Zeeman interaction with the field produced by the polarized ^{3}He multiplied by an atomic parameter κ_0. The value of κ_0 can be thought of as an enhancement due to attraction of the alkali electron wave function to the ^{3}He nucleus [**?**], which is different for each alkali metal species and slightly temperature dependent.

During the process of optical pumping, the Rb atoms are excited to the $5P_{\frac{1}{2}}$ state by the pump laser. The majority of these atoms are quenched non-radiatively to the ground state by N_2. While in the $5P_{\frac{1}{2}}$ state, Rb atoms can also be excited to the $5P_{\frac{3}{2}}$ state through collisions with other Rb atoms. A small fraction of the excited atoms ($5P_{\frac{1}{2}}$ and $5P_{\frac{3}{2}}$) decay by emitting either a D_1 photon or D_2 photon. The intensity of fluorescence is proportional to the population of excited Rb atoms, and is thus higher

when the Rb polarization is low so more Rb atoms can absorb laser and jump to the excited state. We typically induce Zeeman transitions with an RF coil to lower alkali polarization and detect D_2 photons with a photodiode behind a D_2 filter. The highest amount of D_2 photons is detected when the RF frequency is exactly equal to the Zeeman transition frequency.

1.3.2 The Breit-Rabi Equation

The Zeeman energy levels of ground state (L = 0) can be described with the Breit-Rabi equation[**?**]

$$E_{F=I\pm1/2,m_F} = -\frac{h\Delta\nu_{hfs}}{2(2I+1)} - \mu_N g_I B m_F \pm \frac{h\Delta\nu_{hfs}}{2}\sqrt{1+\frac{4m_F x}{2I+1}+x^2} \tag{1.25}$$

where

$$x = (g_I\mu_N - g_s\mu_B)\frac{B}{h\Delta\nu_{hfs}} \tag{1.26}$$

B is the magnetic field, $\Delta\nu_{hfs}$ is the hyperfine splitting frequency, I is the nuclear spin, g_I and g_s are the g factors of nuclear and electron spin, μ_N and μ_B are the nuclear and Bohr magneton, respectively.

The Zeeman transition frequency of $m_F \to m_F - 1$ is

$$\begin{aligned}\nu_{m_F\to m_{F-1}} &= \frac{E_{F,m_F} - E_{F,m_F-1}}{h} \\ &= -\frac{g_I\mu_N B}{h} \pm \frac{\Delta\nu_{hfs}}{2}\left(\sqrt{1+\frac{4m_F}{2I+1}x+x^2} - \sqrt{1+\frac{4m_F-1}{2I+1}x+x^2}\right)\end{aligned} \tag{1.27}$$

The second term is much greater than the first term under our operating conditions, so the sign of the frequency $\nu_{m_F \to m_{F-1}}$ depends on the second term only. If we focus on the $F = I + \frac{1}{2}$ hyperfine manifold, the transition frequency is

$$\nu_{m_F \to m_{F-1}} = -\frac{g_I \mu_N B}{h} + \frac{\Delta\nu_{hfs}}{2}\left(\sqrt{1 + \frac{4m_F}{2I+1}x + x^2} - \sqrt{1 + \frac{4m_F - 1}{2I+1}x + x^2}\right) \tag{1.28}$$

1.3.3 Shift of Zeeman Frequency

Under our operating condition, the size of Zeeman splitting is much less than hyperfine splitting, which makes x a small number. The Taylor expansion of Eq. 1.28 is

$$\begin{aligned}\nu_{m_F \to m_{F-1}} =& -\frac{g_I \mu_N B}{h} \\ &+ \frac{\Delta\nu_{hfs}}{2}\left(\frac{2x}{2I+1} - \frac{2(2m_F - 1)x^2}{(2I+1)^2} + \frac{(-(2I+1)^2 + 4 - 12m_F + 12m_F^2)x^3}{(2I+1)^3} + \cdots\right)\end{aligned} \tag{1.29}$$

with the approximation

$$g_s \mu_B \gg g_I \mu_N \tag{1.30a}$$

$$x \approx -\frac{g_s \mu_B B}{h \Delta\nu_{hfs}} \tag{1.30b}$$

then to the lowest order approximation, the shift of $\nu_{m_F \to m_{F-1}}$ due to a small effective field ΔB ($\Delta B \ll B$) from polarized ^{3}He is

$$\Delta\nu_{m_F\to m_{F-1}} = -\frac{g_s\mu_B}{h(2I+1)}\Delta B\left[1+2(2m-1)\frac{g_s\mu_B B}{h\Delta\nu_{hfs}(2I+1)}\right.$$
$$\left.+6\left(-\frac{(2I+1)^2}{4}+1-3m+3m^2\right)\left(\frac{g_s\mu_B B}{h\Delta\nu_{hfs}(2I+1)}\right)^2+\cdots\right] \tag{1.31}$$

Usually the pumping chamber is spherical, the magnetic field produced inside a uniformly magnetized sphere is [**?**]

$$\Delta\boldsymbol{B} = \frac{2}{3}\mu_0\boldsymbol{M} \tag{1.32}$$

where μ_0 is the vacuum permeability, $\boldsymbol{M}$ is the magnetization of ^{3}He,

$$\boldsymbol{M} = \boldsymbol{\mu_K}[\mathrm{He}]P, \tag{1.33}$$

μ_K is the magnetic moment of ^{3}He, [He] is its density, and P is its polarization. As we mentioned before, as a result of the Fermi-contact interaction $\alpha\mathbf{K}\cdot\mathbf{S}$ between the nuclear spin $\mathbf{K}$ of the noble gas nucleus and the electron spin $\mathbf{S}$ of the alkali metal atom, the effective magnetic field felt by alkali metal due to the polarized ^{3}He nuclei is κ_0 [**?**]:

$$\boldsymbol{\Delta B} = \frac{2}{3}\kappa_0\mu_0\boldsymbol{\mu_K}[\mathrm{He}]P \tag{1.34}$$

The enhancement factor κ_0 was measured by Romalis and Cates in 1998 with an error of 1.5% [**?**]

$$\kappa_0^{Rb-^3He} = 4.52 + 0.00934[T(^\circ C)] \tag{1.35}$$

then it was measured by Babcock *et al.* in 2005 [**?**]

$$\kappa_0^{Rb} = 6.39 + 0.00914[T - 200(^\circ C)] \tag{1.36a}$$

$$\kappa_0^{K} = 5.99 + 0.0086[T - 200(^\circ C)] \tag{1.36b}$$

$$\kappa_0^{Na} = 4.84 + 0.00914[T - 200(^\circ C)] \tag{1.36c}$$

The two results agree within the error. Thus we can calculate ^{3}He polarization with the EPR frequency shift.

1.3.4 Experimental Methods

1.3.4.1 Overview

Under operating conditions typical when using a polarized ^{3}He target, hybrid cells with mixture of Rb and K are used. The vapor density of K is around 6 times as that of Rb, we typically induce the ^{39}K transition corresponding to $m_F = 2 \rightarrow m_F = 1$ (assuming the angular momentum of laser photons is +1), which lowers the K polarization. The Rb-K spin-exchange rate is fast enough that the Rb is depolarized almost instantly. This allows more Rb atoms to absorb laser and be excited to the $5P_{\frac{1}{2}}$ state which in turn produces more D_2 fluorescence. The D_2 fluorescence is at maximum intensity when the RF frequency is on resonance for the Zeeman transition.

We first locate the frequency with a frequency-modulated (FM) sweep, and set the RF frequency to the found value. The RF is locked to the frequency that induces maximum D_2 light using a proportional-integral feedback circuit (P.I. box). This frequency is referred to as the EPR frequency and is measured with a frequency

counter. To separate the frequency-shifting effect of polarized ^{3}He from other sources that may affect the transition frequency, we flip the ^{3}He magnetization by performing AFP using an RF frequency sweep. A frequency sweep is chosen rather than a holding field sweep to keep external magnetic field constant, thus reducing factors that affect Zeeman splitting size. No signal is recorded during theses sweeps, as the varying frequency would affect the amplitude of AFP signals. By comparing the frequency measured before and after the flip, together with the real temperature inside the pumping chamber, we can calculate the ^{3}He polarization. We typically take AFP measurements (in our usual way using a magnetic field sweep) right before and after the relatively quick EPR measurement, so that a calibration constant that translates AFP signal size to ^{3}He polarization can be calculated.

1.3.4.2 Locating Zeeman Transition Frequency

The P.I. box only works well in locking the EPR frequency to the $m_F = 2 \rightarrow m_F = 1$ K transition when the EPR frequency is close to the transition. Thus, the first step in EPR measurements is to locate the Zeeman transition. A frequency-modulated (FM) sweep is performed through a range that covers the Zeeman transition, the range is known from experience or calculation and the P.I. box remains off during the sweep.

The RF frequency is generated by a voltage-controlled oscillator (VCO). The D_2 fluorescence is detected with the photodiode and recorded during the sweep. The RF is frequency-modulated by a 200Hz signal, and the VCO output at any moment during the sweep can be described as:

$$V_{FM}(t) = V_{C0} \sin\left(2\pi[f_c + D_f \sin\left(2\pi f_m t + \phi_m\right)]t + \phi_c\right) \tag{1.37}$$

where V_{C0} is the amplitude of the sweeping RF frequency (carrier), f_c is the RF frequency that is being swept through a set range, D_f is the peak frequency deviation, f_m is the modulating frequency (200Hz in our case), and ϕ_m and ϕ_c are the phase of the modulation frequency and carrier frequency, respectively. Thus, the RF frequency is

$$f_{FM}(t) = f_c(t) + D_f \sin(2\pi f_m t + \phi_m) \tag{1.38}$$

where $f_c(t)$ emphasizes the RF frequency is sweeping over time.

The D_2 light intensity can be described with a Lorentzian function:

$$I(f(t)) = \frac{I_0}{(f_{FM}(t) - f_0)^2 + \Gamma^2} \tag{1.39}$$

where f_0 is the Zeeman transition frequency, Γ is the line width. Keeping the first order term of the Taylor expansion of Eq. 1.39, the D_2 light intensity is

$$I(f(t)) = I(f_c(t)) + \frac{\partial I}{\partial f}\Big|_{f=f_c(t)} D_f \sin(2\pi f_m t + \phi_m) \tag{1.40}$$

A lock-in amplifier is used to select only the f_m term to reduce the noise, which is proportional to the derivative of the Lorentzian function multiplied by a sine function. The FM sweep line crosses zero when the RF frequency is equal to the Zeeman transition frequency (peak of the Lorentzian function), which produces the maximum D_2 light intensity. The region between the lowest and highest points of the derivative line is fitted to a line, and the zero-crossing point of the line is used as the Zeeman transition frequency. Fig. 1.5 shows an FM sweep.

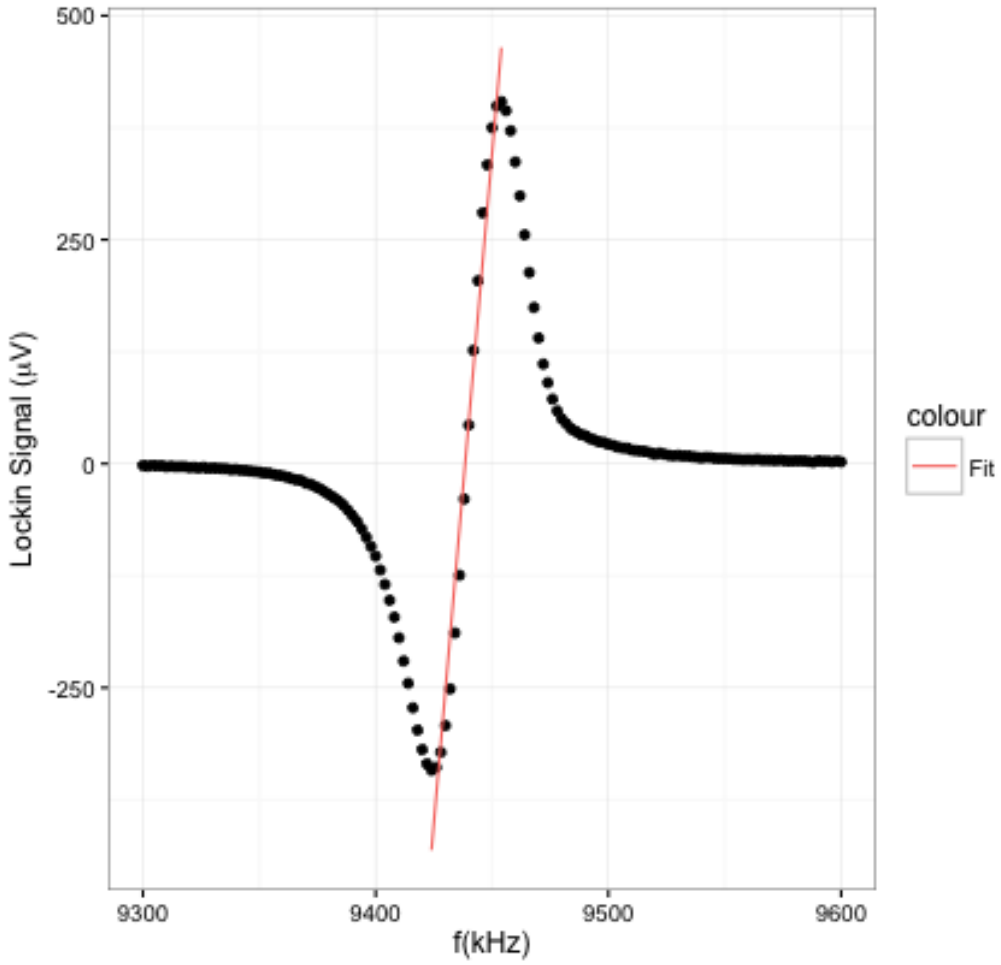

Figure 1.5: A typical FM sweep on a hybrid cell. The central region between the minimum and maximum is fitted to a line. The zero crossing point corresponds to the Zeeman transition frequency.

1.3.4.3 EPR Spin Flip Process

After the transition frequency is located, the VCO frequency is first set to it and then locked with a proportional-integral feedback circuit (P.I. box). The circuit is shown in Fig. 1.6.

The output of the lock-in amplifier serves as an error signal and the input to the

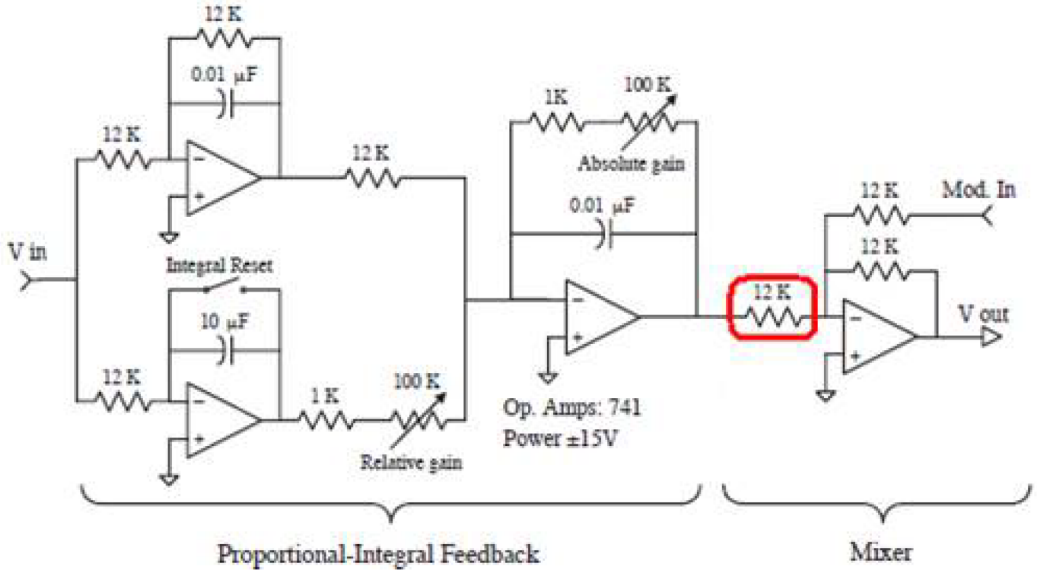

Figure 1.6: The same P.I. circuit that was first used by Romalis in our lab. The drawing was then corrected by Peter Dolph.[?]

P.I. box. The output of the P.I. box is thus forced to a condition that minimizes the error signal and keeps the VCO centered on the resonant frequency.

Because the EPR frequency is also affected by sources other than the polarized ^{3}He such as the holding field and earth field, we flip the ^{3}He spins by sweeping the frequency while keeping the holding field unchanged. The contribution from the flipped spins has the opposite sign while other factors still contribute in the same way, which allows us to extract the change of Zeeman transition frequency due to polarized ^{3}He, and consequently, calculate the polarization. We typically let the cell polarization reach saturation before performing EPR measurements. AFP measurements are taken right before and after the EPR measurements for calculating the calibration constant (the ratio between polarization and AFP signal size). Fig. 1.7 shows a typical EPR spin flip process.

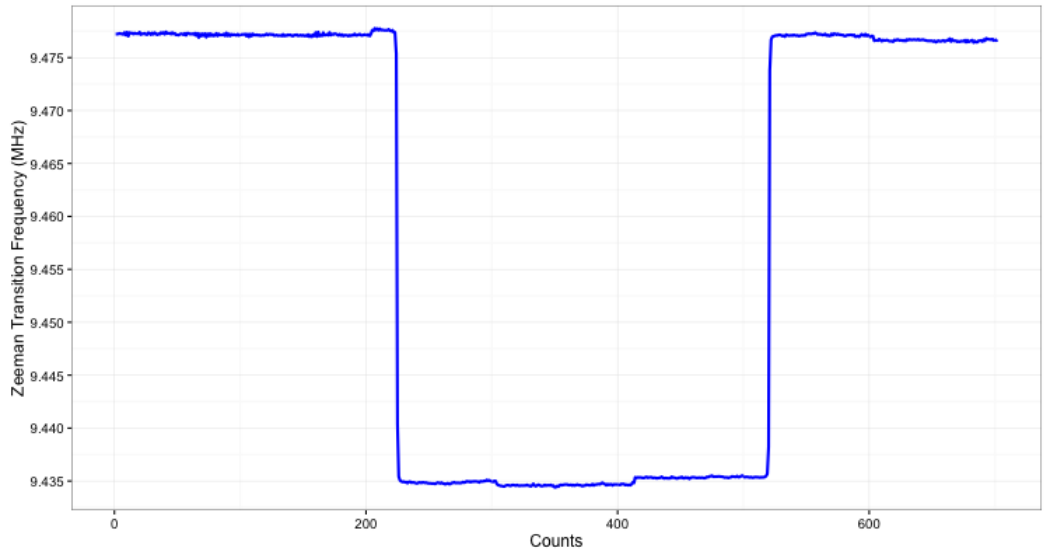

Figure 1.7: An EPR measurement for a hybrid cell at 235°C.

The spins are flipped around 200 mark, and flipped back around 500 mark.

Under normal operating conditions for a double-chambered cell, the pumping chamber is heated to around 170°C or 235°C depending on if the cell is hybrid, while the target chamber and transfer tube remain at room temperature. The temperature difference causes differences in gas densities and affects the AFP signal size. The temperature controller of the oven only maintains the surface temperature of the pumping chamber at a set temperature, but the gas inside the pumping chamber is always hotter due to absorption of laser energy. The enhancement factor κ_0 is also slightly temperature dependent which may be underestimated by $\sim$4% when using the surface temperature as the gas temperature. Dolph described a method we referred to as a "temperature test" to extract gas temperature inside the pumping chamber in detail in his thesis [**?**]. In a temperature test, we take AFP measurements when the laser is blocked and unblocked multiple times. With the assumptions that the change of gas densities due to absorption of laser and AFP losses are the only reasons for the

difference in signal size, and the temperature measured by RTDs on the exterior of the pumping chamber truly reflects the gas temperature when laser is blocked, one can calculate the inside temperature when laser is unblocked.

1.4 Pulsed Nuclear Magnetic Resonance

Adiabatic Fast Passage has been the main technique used in our lab for monitoring relative ^{3}He polarization during various studies. In an AFP measurement, all ^{3}He spins are flipped by sweeping the holding field while applying an RF field. As discussed by Chapter 5, we have been exploring the possibility of replacing conventional glass windows with metal end windows for future experiments planned during the 12 GeV era. Because of the lack of studies on spin relaxation of polarized ^{3}He on metal surfaces, various test cells made with large metal parts as well as glass parts are being studied in our lab. The inclusion of metal parts immediately renders AFP almost useless because of effects such as Eddy currents. Thus, we have been using Pulsed Nuclear Magnetic Resonance (PNMR) for monitoring polarization when studying cells that include metal parts.

1.4.1 The Rotating Coordinate System

In a PNMR measurement, a short pulse of RF frequency is applied to a small localized portion of ^{3}He gas. The RF frequency is tuned to be on resonance at the Larmor frequency of the holding field. As discussed before with AFP, in the rotating coordinate system, there will be an effective field due to rotation that exactly cancels the holding field which we assume to be in the z direction. Thus the z component

of the effective field is zero and there is a non-zero constant transverse component which we will call B_1. The nuclear spins will precess along B_1 and end up at an angle away from z axis:

$$\alpha = \gamma B_1 \Delta t \tag{1.41}$$

where α is the angle (tip angle), γ is the gyromagnetic ratio, and Δt is the RF pulse duration.

1.4.2 Free Induction Decay

At the end of the RF pulse, the tipped spins will have a transverse component equal to the magnetization multiplied by $\sin\alpha$. The spins continue to precess along the holding field and the transverse component will induce a signal in the pickup coils (wrapped around the transfer tube as shown in Fig. 1.8) whose axis is perpendicular to the holding field.

In addition to precession, the spins are affected by two types of relaxation processes. The first type is called the spin-lattice relaxation, it describes the rate at which the longitudinal component of magnetization approaches the thermodynamic equilibrium value. It is characterized by the spin-lattice relaxation time constant T_1. The rate of change of the longitudinal component is

$$\dot{M}_z = -(M_z - M_0)/T_1 \tag{1.42}$$

where M_0 is the thermodynamic equilibrium magnetization. Solving the differential equation gives

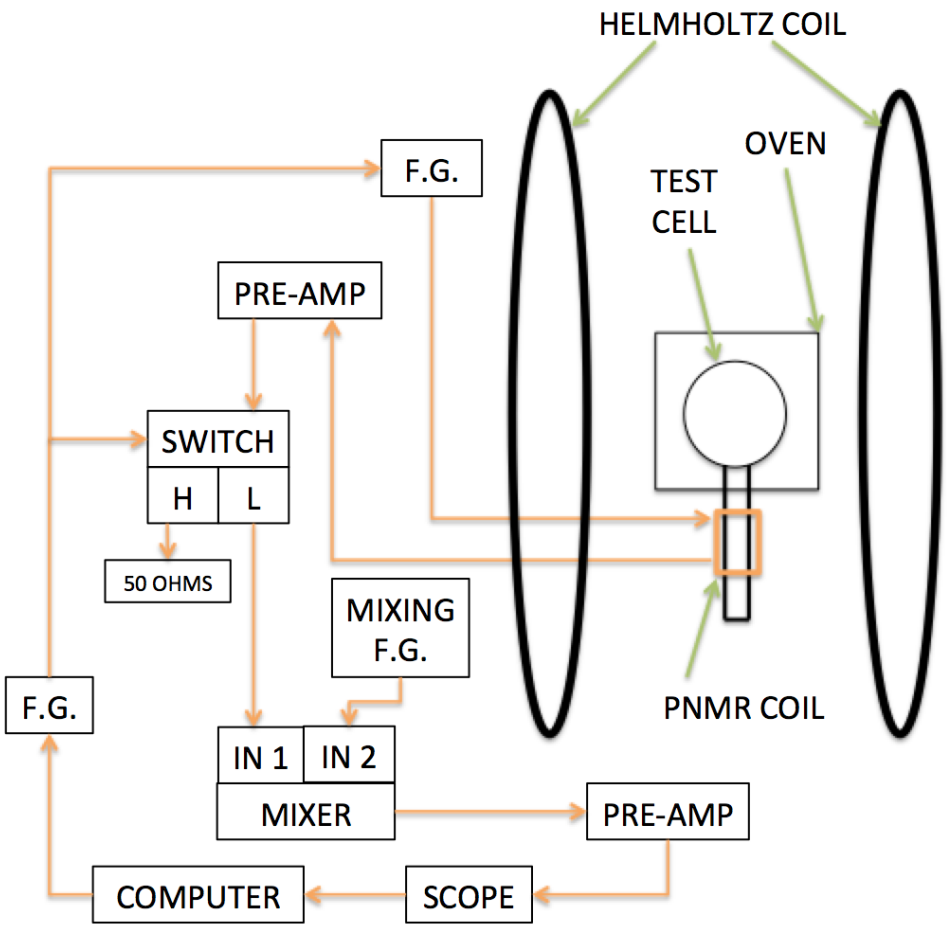

Figure 1.8: PNMR setup.

$$M_z(t) = M_0 - [M_0 - M_z(0)]\, e^{-t/T_1} \tag{1.43}$$

The name spin-lattice relaxation refers to the process in which the spins transfer energy to surrounding, thereby restoring their equilibrium state.

The second relaxation process is relaxation in the transverse plane, which is also referred to as the T_2 relaxation and was historically called "spin-spin relaxation". The transverse component of magnetization decays because random fluctuations of

the holding field cause different moments to precess at different rates. This is the T_2 process. Normally, the dominating relaxation effect however, is another dephasing process due to holding field inhomogeneities over the volume of the cell.

The measured transverse relaxation rate of the tipped spins is the result of all these effects combined:

$$\frac{1}{T_2^*} = \frac{1}{T_2} + \gamma \Delta B_0 \tag{1.44}$$

where ΔB_0 is the variation in the holding field. $\gamma \Delta B_0$, the dominant term, is a spread in Larmor frequencies $\Delta\omega_0$, which causes spin-spin dephasing in a characteristic time of $1/\Delta\omega_0$.

The time evolution of the nuclear magnetization $\mathbf{M}$ can be described by the Bloch equations [**?**]:

$$\frac{\partial M_x(t)}{\partial t} = \gamma \left(\boldsymbol{M(t)} \times \boldsymbol{B(t)}\right)_x - \frac{M_x(t)}{T_2^*} \tag{1.45a}$$

$$\frac{\partial M_y(t)}{\partial t} = \gamma \left(\boldsymbol{M(t)} \times \boldsymbol{B(t)}\right)_y - \frac{M_y(t)}{T_2^*} \tag{1.45b}$$

$$\frac{\partial M_z(t)}{\partial t} = \gamma \left(\boldsymbol{M(t)} \times \boldsymbol{B(t)}\right)_z - \frac{M_z(t)}{T_1} \tag{1.45c}$$

where γ is the gyromagnetic ratio and the cross products are the precession terms, the last terms in each equation represent the decaying and dephasing of each component. The precessing spin magnetization generates a signal in the pickup coils that decays with time. This is called free induction decay, the induced signal is typically described by

$$V(t) = A\omega_0 \sin\alpha \sin(\omega_0 t + \phi) e^{-t/T_2^*} \tag{1.46}$$

where A is just a constant, ω_0 is the Larmor frequency for the holding field, α is the tip angle, T_2^* is the measured decay time constant. For our metal test cells, depending on the location of the pickup coils and the field setup, T_2^* varies between several milliseconds to more than 300 milliseconds.

1.4.3 Experimental Methods

Our PNMR setup is shown in Fig. 1.8. The Labview program on the computer controlled the timing of a gate signal that was fired from the first function generator (F.G.). The gate signal was fed to the back of the second function generator and triggered it to produce a short pulse. The second function generator sent out RF pulse with pre-set amplitude, duration and frequency only when the gate signal was of voltage higher than the threshold. The frequency of the RF pulse was carefully tuned to be at the Larmor frequency of the holding field.

The pulse was sent from the function generator to a coil wrapped directly on a small portion of the cell. The spins in the proximity of the coil were exposed to the pulse and tipped by an angle which depended on the amplitude and the duration of the pulse. In the rotating frame, the effective field B_1 caused the spins to precess around it (as discussed before), the precession frequency was γB_1 so the angle the spins rotate by (tip angle) can be calculated by:

$$\alpha = \gamma B_1 \Delta t \tag{1.47}$$

where γ is the gyromagnetic ratio, the effective field B_1 is directly proportional to the amplitude of the RF pulse, and Δt is the duration of the pulse. Ideally, a 90° tip angle would result in the maximum signal, but it had not been the case for us most of the time. The coils were normally wrapped on the transfer tube of the cell which was off the center of the holding field and exposed to relatively large holding field inhomogeneities. Different groups of spins contributed to the FID signal also saw different values of B_1. The details of how we measure the test cells will be discussed in later chapters. As a result, the spins to precessed at different rates, and the dephasing became more significant with longer pulse duration and larger tip angle, which led to non-optimal signals. Exact tip angles of specific group of spins depended on location, a typical effective tip angle for the whole region would be between 30° and 45°.

After the spins were tipped away from z axis, they precessed around the holding field and induced a signal in the detection coil. The signal was amplified by a low noise pre-amplifier first and then went through an isolation switch. The switch only let signal pass when the controlling gate voltage was low, thus stopped the RF pulse from coming back through the detection circuit. The signal was at the Larmor frequency, and was mixed with another frequency after the switch. The mixing frequency was only slightly different from the Larmor frequency, the output of the mixer had both the sum of the two frequencies and the difference. A second pre-amplifier was used to select and amplify the lower of the two frequencies while filtering out high frequency noises. The final output was displayed on a oscilloscope and collected by the Labview program on the computer. Fig. 1.9 shows a PNMR measurement with around 150 ms decay time constant.

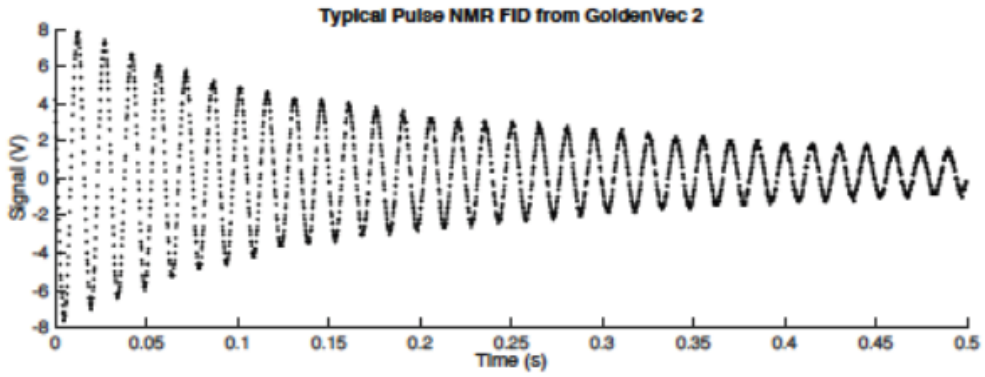

Figure 1.9: A PNMR signal taken with gold coated test cell.

The tip angle was measured with a short sequence of FID signals. Theoretically the tip angle can be calculated with Eq. 1.47. But because of inhomogeneities and other factors, the calculation serves as only an estimate in practice and it was often more accurate and convenient to measure the tip angle directly. We took several PNMR measurements in quick succession with the same RF pulse settings. After every pulse, the transverse component of the spins quickly decayed and dephased, leaving only the longitudinal component which was equal to $\cos\alpha$ times the original magnetization. The intervals between measurements were short enough so that T_1 can be safely ignored. The series of measurements also needed to be performed on the same portion of the gas (i.e. the same group of spins tipped by the first pulse), thus it was important to know that the self-diffusion of ^{3}He was significantly slower than the sampling rate. The self-diffusion coefficient of ^{3}He at 300K is [**?**]

$$D = \frac{1440(80)\text{torr}}{\text{P}}\text{cm}^2/\text{s} \tag{1.48}$$

which is roughly 1.89 cm^2/s at 760 torr (the test cells normally contained around 1 atm of ^3He). The diffusion length is described by

$$l = 2\sqrt{Dt} \tag{1.49}$$

Thus in one second, the gas moved around 2.75 cm through self-diffusion. For this reason, we only took 2 or 3 PNMR measurements to calculate the tip angle. As additional measurements would have given enough time for the tipped spins from the first PNMR and the surrounding spins to mix.

Since only the longitudinal component of the tipped spins were preserved, the amplitude of the i_{th} PNMR was

$$V_i = V_0 cos^{i-1}\alpha \tag{1.50}$$

where V_0 is the induced signal in the first PNMR. We could then use this equation to calculate the effective tip angle α.

Bibliography

[1] High-performance nuclear-polarized ^{3}He targets for electron scattering based on spin-exchange optical pumping. *PhD thesis, University of Virginia*, 2010.

[2] A. Abragam. *Principles of Nuclear Magnetism.*

[3] E. Babcock, I. A. Nelson, S. Kadlecek, and T. G. Walker. ^{3}He polarization-dependent epr frequency shifts of alkali-metal$^{\smile 3}$He pairs. *Phys. Rev. A*, 71:013414, Jan 2005.

[4] F. Bloch. Nuclear induction. *Phys. Rev.*, 70:460–474, Oct 1946.

[5] G. Breit and I. I. Rabi. Measurement of nuclear spin. *Phys. Rev.*, 38:2082–2083, Dec 1931.

[6] G. D. Cates, S. R. Schaefer, and W. Happer. Relaxation of spins due to field inhomogeneities in gaseous samples at low magnetic fields and low pressures. *Phys. Rev. A*, 37:2877–2885, Apr 1988.

[7] G. D. Cates, D. J. White, T.-R. Chien, S. R. Schaefer, and W. Happer. Spin relaxation in gases due to inhomogeneous static and oscillating magnetic fields. *Phys. Rev. A*, 38:5092–5106, Nov 1988.

[8] I. Delstar Metal Finishing. *https://www.delstar.com/electropolishing*.

[9] R. L. Gamblin and T. R. Carver. Polarization and relaxation processes in he^3 gas. *Phys. Rev.*, 138:A946–A960, May 1965.

[10] J. Jackson. *Classical Electrodynamics*.

[11] D. Matyas. Characterizing ^{3}he nuclear spin relaxation in vessels of glass and metal. *Master thesis, University of Virginia*, 2016.

[12] I. I. Rabi, N. F. Ramsey, and J. Schwinger. Use of rotating coordinates in magnetic resonance problems. *Rev. Mod. Phys.*, 26:167–171, Apr 1954.

[13] M. L. R.Barbe and F. Laloe. Experimental verifications - measurement of the he3 self-diffusion coefficient. 35:935–951, 1974.

[14] M. V. Romalis and G. D. Cates. Accurate ^{3}He polarimetry using the rb zeeman frequency shift due to the Rb$-^3$He spin-exchange collisions. *Phys. Rev. A*, 58:3004–3011, Oct 1998.

[15] M. V. Romalis, E. Miron, and G. D. Cates. Pressure broadening of rb d_1 and d_2 lines by ^{3}he, ^{4}he, n_2, and xe: line cores and near wings. *Phys. Rev. A*, 56(6), 1997.

[16] L. D. Schearer and G. K. Walters. Nuclear spin-lattice relaxation in the presence of magnetic-field gradients. *Phys. Rev.*, 139:A1398–A1402, Aug 1965.

[17] T. G. Walker and W. Happer. Spin-exchange optical pumping of noble-gas nuclei. *Rev. Mod. Phys.*, 69:629–642, Apr 1997.

[18] Y. Zheng. Low field mri and the development of polarized nuclear imaging (pni)-a new imaging modality, 2015.

Appendix A

Appendix title

This is Appendix A.

You can have additional appendices too (*e.g.*, `apdxb.tex`, `apdxc.tex`, *etc.*). If you don't need any appendices, delete the appendix related lines from `thesis.tex` and the file names from `Makefile`.